HHS Public Access

Author manuscript

J Am Chem Soc. Author manuscript; available in PMC 2019 September 16.

Published in final edited form as:

J Am Chem Soc. 2019 August 14; 141(32): 12475–12480. doi:10.1021/jacs.9b05195.

Shortwave Infrared Imaging with J-Aggregates Stabilized in Hollow Mesoporous Silica Nanoparticles

Wei Chen[#,†,‡], **Chi-An Cheng**[§,†,‡], **Emily D. Cosco**[#,⊥,‡], **Shyam Ramakrishnan**[⊥], **Jakob G. P. Lingg**[⊥], **Oliver T. Bruns**[*,⊥], **Jeffrey I. Zink**[*,#,†], **Ellen M. Sletten**[*,#,†]

[#]Department of Chemistry and Biochemistry, University of California, Los Angeles, 607 Charles E. Young Drive East, Los Angeles, California 90095, United States

[§]Department of Bioengineering, University of California, Los Angeles, 607 Charles E. Young Drive East, Los Angeles, California 90095, United States

[†]California NanoSystems Institute, University of California, Los Angeles, 607 Charles E. Young Drive East, Los Angeles, California 90095, United States

[⊥]Helmholtz Pioneer Campus, Helmholtz Zentrum München, D-85764 Neuherberg, Germany

Abstract

Tissue is translucent to shortwave infrared (SWIR) light, rendering optical imaging superior in this region. However, the widespread use of optical SWIR imaging has been limited, in part, by the lack of bright, biocompatible contrast agents that absorb and emit light above 1000 nm. J-Aggregation offers a means to transform stable, near-infrared (NIR) fluorophores into red-shifted SWIR contrast agents. Here we demonstrate that J-aggregates of NIR fluorophore IR-140 can be prepared inside hollow mesoporous silica nanoparticles (HMSNs) to result in nanomaterials that absorb and emit SWIR light. The J-aggregates inside PEGylated HMSNs are stable for multiple weeks in buffer and enable high resolution imaging *in vivo* with 980 nm excitation.

Optical imaging with shortwave infrared (SWIR, 1000–2000 nm) light has emerged as a powerful method of fluorescence imaging in animals due to the superior resolution and contrast one can achieve with low energy light (Figure 1A).[1] A primary challenge with SWIR imaging is the development of bright, biocompatible, SWIR contrast agents.[2] Originally, the advantageous qualities of imaging in the SWIR region were showcased with carbon nanotubes,[3] quantum dots,[4] and rare earth nanomaterials.[5] In efforts to set the stage for clinical translation, the past three years have seen a focus on the synthesis of nontoxic, SWIR-emissive organic fluorophores.[6] This work has significantly expanded the suite of fluorophores that emit above 1000 nm; however, challenges remain in the stability, delivery,

[*]Corresponding Authors: Sletten@chem.ucla.edu, Zink@chem.ucla.edu, Oliver.bruns@helmholtz-muenchen.de.
[‡]These authors contributed equally.

The authors declare no competing financial interest.

Supporting Information

The Supporting Information is available free of charge on the ACS Publications website at DOI: 10.1021/jacs.9b05195.
All experimental procedures, Figures S1–S22, Tables S1–S3, Schemes S1 and S2, Notes S1–S4 (PDF)

and brightness of SWIR dyes. Consequently, we looked to explore an alternative avenue to create SWIR organic materials: J-aggregation.

J-Aggregation is the slip-stacked alignment of chromophores that leads to constructive coupling of the excited state transition dipoles (Figure 1B).[7] The photophysical consequences of J-aggregation are bathochromically shifted absorption and emission spectra, narrow absorption and emission bands with small Stokes shifts, enhanced absorbance coeffcients (ε), and shortened fluorescence lifetimes which can result in enhanced quantum yields (Φ_F) and cycling rates. Many J-aggregate characteristics are beneficial qualities for *in vivo* imaging: red-shifted absorption and emission spectra will enable significant depth penetration during both the excitation and image acquisition,[2,8] narrow bands can facilitate multi plexed imaging, and increased ε will result in bright materials. Despite the significant photophysical advantages J-aggregates typically have over the monomer, there are few reports of employing J-aggregates for *in vivo* imaging due to the diffculty in obtaining and stabilizing the necessary chromophore alignment in complex settings.[9]

Nanostructures can sequester and protect payloads, rendering nanomaterials a promising approach toward stabilizing J-aggregates *in vivo*. In 2016, Zheng and co-workers performed image-guided surgery with porphyrin lipids that formed J-aggregates upon self-assembly into nanovesicles.[10] The following year, Xu and co-workers prepared pyrrolopyr-role cyanine J-aggregate-containing polymer micelles, which could be visualized after subcutaneous injection.[11] In work recently published, Fan and co-workers reported a squaraine J-aggregate, stabilized in polymeric micelles, for SWIR image-guided photothermal therapy.[12] Each of these reports utilizes self-assembled organic nanomaterials, [13] which are prone to disassembly when diluted in the presence of hydrophobic biomolecules, leading to destabilization of the J-aggregate.[14] Here, we employ robust, biocompatible, hollow mesoporous silica nanoparticles to stabilize and protect SWIR-emissive J-aggregates of IR-140 for in vivo imaging (Figure 1C,D).

Hollow mesoporous silica nanoparticles (HMSNs) have 2–4 nm pores that open into a large, 10–200 nm cavity, allowing these nanostructures to carry significant cargo.[15] The surfaces of the HMSNs can be modified to alter the biodistribution of the nanoparticles.[16] Consequently, there are numerous reports of HMSNs as the core scaffold of multifunctional materials. [15a,16b,17] Included in these studies are the loading or conjugation of visible[18] and near-infrared[15a,19] fluorophores and administering the resulting nanomaterials for imaging. However, the controlled assembly of J-aggregates in HMSNs has yet to be demonstrated.

To realize SWIR-emissive J-aggregates inside HMSNs, we utilized the heptamethine dye IR-140 (1). IR-140 is a commercially available NIR fluorophore ($\lambda_{max,abs}$ = 826 nm, $\lambda_{max,em}$ = 875 nm) that has been applied as a photo-polymerization initiator,[20] fluorescent payload,[21] component of plasmonic arrays,[22] as well as a Raman[23] and two-photon[24] imaging agent. In 2016, Wang and Weiss reported that introduction of IR-140 to glutathione-coated quantum dots results in J-aggregate formation with two aggregates observed: J1, ($\lambda_{max,abs}$ = 965 nm, nonemissive) and J2 ($\lambda_{max,abs}$ = 1040 nm, λ = 1047 nm).[25] We envisioned that similar IR-140 J-aggregates could be formed on the negatively charged pores

and inner surface of HMSNs. Further, once the aggregates were assembled inside the particles, the hydrophobic nature of IR-140 would make them unlikely to disassemble in aqueous environments, rendering J-aggregates stable *in vivo*.

We prepared HMSNs by synthesizing a mesoporous silica coating on a Stöber sphere core that was subsequently removed via etching with sodium carbonate (Scheme S1, Figure S1). The HMSNs were treated with varying amounts of IR-140 in different solvents (Figure 2A). J-Aggregate formation was assayed by UV/vis/NIR spectroscopy evaluating loss of monomeric IR-140 at 826 nm and formation of the J-aggregates at 965 nm (J1) and 1040 nm (J2). Upon optimization, we found that SWIR J-aggregates could be obtained when IR-140 dissolved in dimethyl sulfoxide (DMSO) was combined with HMSNs and washed. The washing procedure proved essential for obtaining the desired J2 aggregate formation (Figures 2B and S2), with gentle PBS washes yielding the largest amount of the desired J2 aggregate (dark blue, Figure 2B). When these optimized conditions were repeated on Stöber spheres that did not have pores or an inner surface for IR-140 to associate with, only a small J-band was observed (Figure 2B, gray line, Figure S3). Similar results were obtained when loading was performed on mesoporous silica coated Stöber spheres (Figure S2). These control experiments (Figure S5) suggest that the majority of IR-140 is protected inside the HMSN cavity. Through analysis of IR-140 collected after the washing procedures, we calculated the loading of IR-140 to be ~10^3 molecules/particle (Figure S6, Note S1).

The HMSNs were further characterized through transmission electron microscopy (TEM), which showed ~85 nm particles with a distinct cavity and pores (Figure 2C). The pore size was quantified to be 3.2 nm through nitrogen adsorption experiments (Figure S4). While the pores are clearly visible in the TEM of the empty HMSNs, they are darkened after treatment with IR-140 (Figure 2D), suggesting the presence of IR-140. Control experiments in which HMSNs were subjected to PBS washing procedures but no IR-140 show no change in contrast of the pores upon TEM analysis (Figure S7).

After confirming that the HMSNs could facilitate J-aggregation of IR-140, we modified the surface with poly-(ethylene glycol) (PEG) such that they could be suspended in aqueous media. This was accomplished by loading HMSNs that had undergone surface silanization with (3-aminopropyl)-triethoxysilane (APTS) prior to Stöber sphere and surfactant removal (Scheme S2). This procedure resulted in HMSNs that were positively charged on the outside but still contained a negatively charged interior to associate with the cationic IR-140.[26] Nitrogen adsorption data (Figure S4) also suggests that the pores are not modified with APTS.[27] The introduction of IR-140 into the HMSNs-APTS proceeded similarly to the HMSNs, yielding analogous loading of IR-140 and a higher ratio of J2:J1 (Figure S8). Control experiments performed with Stöber spheres treated with APTS support that IR-140 is protected on the interior of the HMSNs (Figures S3 and S5). After loading, a 23 kDa PEG-carboxylate was conjugated to the amines present on the outer surface of the HMSNs-APTS using carbodiimide chemistry (Scheme S2). Successful PEG conjugation was verified by changes in hydrodynamic diameter and ζ-potential (Figures S9 and S10).

We evaluated the photophysical properties of the PEGylated HMSNs (HMSNs-PEG) containing IR-140 in comparison to IR-140 in solution as the monomer and J-aggregate

(Figure 3A). Monomeric IR-140 has been well-characterized;[28] however, the solution J-aggregate of IR-140 had previously not been reported.[29] After screening numerous conditions (Figure S11), we found that 35% DMSO/0.9% NaCl in water afforded formation of the desired SWIR J-aggregate with a $\lambda_{max,abs}$ = 1042 nm, $\lambda_{max,em}$ = 1043 nm, ε = 3.9 × 10^5 M^{-1} cm^{-1}, and Φ_F = 0.01% (Table S1, Notes S2 and S3). The IR-140-containing HMSNs-PEG had similar spectral properties with a $\lambda_{max,abs}$ = 1038 nm, $\lambda_{max,em}$ = 1047 nm, although the absorbance was considerably broader, which we attribute to the presence of other nonemissive aggregate states. When solutions of IR-140 in DMSO, IR-140 in 35% DMSO/0.9% NaCl in water, and IR-140 loaded HMSNs-PEG in PBS were excited with a 980 nm laser, the wavelength to be used for in vivo imaging experiments, the IR-140 J-aggregate in solution and in the particles were similarly emissive, while the monomer was not excited by 980 nm light (Figures 3B and S12).[30] Thus, J-aggregation is essential for SWIR imaging with low energy excitation.

Next, we analyzed the role of the HMSNs in stabilizing IR-140 J-aggregates. Over 2 weeks in PBS at room temperature, we observed only a ~10% decrease in absorbance from the IR-140 loaded HMSNs-PEG and no evidence that the packing of the IR-140 within the nanoparticles was changing (Figures 3C, blue; S13). Comparatively, only ~8% of the J-aggregate in solution remained after 1 day (Figures 3C, red; S13). Not only do the HMSNs stabilize the assembly of the J-aggregate, but they also enhance the photostability. The fluorescence of solutions containing IR-140 J-aggregate in 35% DMSO/0.9% NaCl in water and HMSNs-PEG containing IR-140 J-aggregate in PBS were continually irradiated with a 980 nm laser (97 mW/cm^2) and the fluorescence intensity was measured with an InGaAs camera. The photostability of monomeric IR-140 in DMSO was also evaluated via excitation at 785 nm (97 mW/cm^2). As shown in Figure 3D, the J-aggregates within the HMSNs-PEG are 4-fold more stable than the J-aggregates in solution and ~60-fold more stable than the monomer (Table S2, Note S4). This result is consistent with the use of silica shells to overcome the poor photostability that is characteristic of J-aggregates by limiting the amount of reactive oxygen species that can access the aggregate.[31] Photobleaching experiments in deoxygenated solvents support that the HMSNs protect the IR-140 J-aggregate from reactive oxygen species (Figure S14). Taken together, our data show that the HMSNs are critical for stabilizing J-aggregates to light and solution.

Finally, with bright SWIR-emissive nanoparticles prepared and characterized, we evaluated their biocompatibility and *in vivo* imaging performance. *In vitro* studies showed no cytotoxicity of the IR-140 loaded HMSNs-PEG over 6 h at concentrations up to 200 μg/mL (Figure S15). These data are consistent with other studies regarding mesoporous silica, which is generally considered nontoxic to animals.[26,32] We performed *in vivo* imaging experiments using the IR-140 loaded HMSNs-PEG with excitation at 980 nm and collection from 1000–1700 nm. The SWIR-emissive HMSNs-PEG were intravenously injected into nude mice and the mice were immediately imaged (Figure 4). The HMSNs-PEG rapidly clear from the bloodstream and intense signal can be seen in the lungs, liver, and spleen. Fifty minutes after injection, the signal intensity within these organs remained constant (Figure S16).

In summary, we have presented J-aggregation as an approach to prepare biocompatible, SWIR contrast agents and demonstrated this concept by stabilizing J-aggregates of the NIR fluorophore IR-140 inside HMSNs. The bathochromically shifted absorption and emission and small Stokes shifts of the IR-140 J-aggregate allow imaging with 980 nm excitation and 1000–1700 nm acquisition, providing high resolution *in vivo* images. The modularity of the HMSNs will enable facile exchange of the imaging agent as well as the addition of targeting agents and/or therapeutics, poising these materials to become SWIR theranostics.[33] While we did not observe an enhanced Φ_F with the IR-140 J-aggregate, likely due to disorder or intermolecular vibrations,[34] work is ongoing to access a SWIR J-aggregate that exhibits the superradience phenomena predicted by Kasha.[35] Collectively, the use of J-aggregates stabilized in HMSNs as SWIR imaging agents has the potential to overcome the stability, toxicity, and brightness challenges of contrast agents for this compelling region of the electromagnetic spectrum.

Supplementary Material

Refer to Web version on PubMed Central for supplementary material.

ACKNOWLEDGMENTS

We thank Prof. Matthias Tschöp, Prof. Vasilis Ntziachristos, Dr. Thomas Schwarz-Romond, Uwe Klemm, and all members of the Helmholtz Pioneer Campus and Institute for Biological and Medical Imaging for their support. This work was supported by grants to E.D.C. (NSF GRFP DGE-1144087, Christopher S. Foote Fellowship), O.T.B. (Emmy-Noether-Programm of DFG BR 5355/2-1, Helmholtz Pioneer Campus Institute for Biomedical Engineering), J.I.Z. (Zink student research fund), and E.M.S. (UCLA, Sloan Research Award FG-2018-10855, NIH 1R01EB027172-01).

REFERENCES

(1). (a)Hong G; Antaris AL; Dai H Near-infrared fluorophores for biomedical imaging. Nat. Biomed. Eng 2017, 1, 0010.(b)Carr JA; Aellen M; Franke D; So PTC; Bruns OT; Bawendi MG Absorption by water increases fluorescence image contrast of biological tissue in the shortwave infrared. Proc. Natl. Acad. Sci. U.S. A 2018, 115, 9080–9085. [PubMed: 30150372] (c)Smith AM; Mancini MC; Nie SM Second window for in vivo imaging. Nat. Nanotechnol 2009, 4, 710–711. [PubMed: 19898521]

(2). Thimsen E; Sadtler B; Berezin MY Shortwave-infrared (SWIR) emitters for biological imaging: a review of challenges and opportunities. Nanophotonics 2017, 6, 1043–1054.

(3). Welsher K; Liu Z; Sherlock SP; Robinson JT; Chen Z; Daranciang D; Dai H A route to brightly fluorescent carbon nanotubes for near-infrared imaging in mice. Nat. Nanotechnol 2009, 4, 773–780. [PubMed: 19893526]

(4). (a)Hong G; Robinson JT; Zhang YJ; Diao S; Antaris AL; Wang QB; Dai H In vivo fluorescence imaging with Ag_2S quantum dots in the second near-infrared window. Angew. Chem., Int. Ed 2012, 51, 9818–9821.(b)Bruns OT; Bischof TS; Harris DK; Franke D; Shi Y; Riedemann L; Bartelt A; Jaworski FB; Carr JA; Rowlands CJ; Wilson MWB; Chen O; Wei H; Hwang GW; Montana DM; Coropceanu I; Achorn OB; Kloepper J; Heeren J; So PTC; Fukumura D; Jensen KF; Jain RK; Bawendi MG Next-generation in vivo optical imaging with short-wave infrared quantum dots. Nat. Biomed. Eng 2017, 1,0056. [PubMed: 29119058]

(5). (a)Chen G; Ohulchanskyy TY; Liu S; Law W-C; Wu F; Swihart MT; Agren H; Prasad PN Core/shell NaGdF4:Nd3+/ NaGdF4 nanocrystals with efficient near-infrared to near-infrared downconversion photoluminescence for bioimaging applications. ACS Nano 2012, 6, 2969–2977. [PubMed: 22401578] (b)Naczynski DJ; Tan MC; Zevon M; Wall B; Kohl J; Kulesa A; Chen S; Roth CM; Riman RE; Moghe PV Rare-earth doped biological composites as in vivo shortwave infrared reporters. Nat. Commun 2013, 4, 2199. [PubMed: 23873342]

(6). (a)Yang Q; Ma Z; Wang H; Zhou B; Zhu S; Zhong Y; Wang J; Wan H; Antaris A; Ma R; Zhang X; Yang J; Zhang X; Sun H; Liu W; Liang Y; Dai H Rational design of molecular fluorophores for biological imaging in the NIR-II window. Adv. Mater 2017, 29, 1605497.(b)Cosco ED; Caram JR; Bruns OT; Franke D; Day RA; Farr EP; Bawendi MG; Sletten EM Flavylium polymethine fluorophores for near- and shortwave infrared imaging. Angew. Chem., Int. Ed 2017, 56, 13126–13129.(c)Xu G; Yan Q; Lv X; Zhu Y; Xin K; Shi B; Wang R; Chen J; Gao W; Shi P; Fan C; Zhao C; Tian H Imaging of colorectal cancers using activatable nanoprobes with second near-infrared window emission. Angew. Chem., Int. Ed 2018, 57, 3626–3630.(d)Li B; Lu L; Zhao M; Lei Z; Zhang F An efficient 1064 nm NIR-II excitation fluorescent molecular dye for deep-tissue high-resolution dynamic bioimaging. Angew. Chem., Int. Ed 2018, 57, 7483–7487.(e)Yang Q; Hu Z; Zhu S; Ma R; Ma H; Ma Z; Wan H; Zhu T; Jiang Z; Liu W; Jiao L; Sun H; Liang Y; Dai H Donor engineering for NIR-II molecular fluorophores with enhanced fluorescent performance. J. Am. Chem. Soc 2018, 140, 1715–1724. [PubMed: 29337545] (f)Sheng ZH; Guo B; Hu DH; Xu SD; Wu WB; Liew WH; Yao K; Jiang JY; Liu CB; Zheng HR; Liu B Bright aggregation-induced emission dots for targeted synergetic NIR-II fluorescence and NIR-I photo-acoustic imaging of orthotopic brain tumors. Adv. Mater 2018, 30, 1800766.

(7). (a)Wuerthner F; Kaiser TE; Saha-Moeller CR J-aggregates: From serendipitous discovery to supramolecular engineering of functional dye materials. Angew. Chem., Int. Ed 2011, 50, 3376–3410.(b)J-aggregates; Kobayashi T, Ed.; World Scientific: Singapore, 1996.(c)Jelley EE Spectral absorption and fluorescence of dyes in the molecular state. Nature 1936, 138, 1009–1010. (d)Scheibe G Uber die veranderlichkeit der absorptionsspektren in losungen und die nebenvalenzen als ihre ursache. Angew. Chem 1937, 50, 212–219.(e)Hestand NJ; Spano FC Molecular aggregate photophysics beyond the Kasah Model: Novel design principles for organic materials. Acc. Chem. Res 2017, 50, 341–350. [PubMed: 28145688]

(8). (a)Bashkatov AN; Genina EA; Kochubey VI; Tuchin VV Optical properties of human skin, subcutaneous and mucous tissues in the wavelength range from 400 to 2000 nm. J. Phys. D: Appl. Phys 2005, 38, 2543–2555.(b)Lim YT; Kim S; Nakayama A; Stott NE; Bawendi MG; Frangioni JV Selection of quantum dot wavelengths for biomedical assays and imaging. Mol. Imaging 2003, 2, 50–64. [PubMed: 12926237] (c)Won N; Jeong S; Kim K; Kwag J; Park J; Kim SG; Kim S Imaging depths of near-infrared quantum dots in first and second optical windows. Mol. Imaging 2012, 11, 338–352. [PubMed: 22954148]

(9). Bricks JL; Slominskii YL; Panas ID; Demchenko AP Fluorescent J-aggregates of cyanine dyes: basic research and applications review. Methods Appl. Fluoresc 2018, 6, 012001.

(10). Shakiba M; Ng KK; Huynh E; Chan H; Charron DM; Chen J; Muhanna N; Foster FS; Wilson BC; Zheng G Stable J-aggregation enabled dual photoacoustic and fluorescence nano-particles for intraoperative cancer imaging. Nanoscale 2016, 8, 12618–12625. [PubMed: 26731304]

(11). Yang C; Wang X; Wang M; Xu K; Xu C Robust colloidal nanoparticles of pyrrolopyrrole cyanine J-aggregates with bring near-infrared fluorescence in aqueous media: From spectral tailoring to bioimaging applications. Chem. - Eur. J 2017, 23, 4310–4319. [PubMed: 27918633]

(12). Sun P; Wu Q; Sun X; Miao H; Deng W; Zhang W; Fan Q; Huang W J-aggregate squaraine nanoparticles with bright NIR-II fluorescence for imaging guided photothermal therapy. Chem. Commun 2018, 54, 13395–13398.

(13). Two other J-aggregates have been employed in vivo for photothermal therapy and photoacoustic imaging.(a)Song X; Gong H; Liu T; Cheng L; Wang C; Sun X; Liang C; Liu Z J-aggregates of organic dye molecules complexed with iron oxide nanoparticles for imaging-guided photothermal therapy under 915 nm light. Small 2014, 10, 4362–4370. [PubMed: 24976309] (b)Dumani DS; Brecht H-P; Ivanov V; Deschner R; Harris JT; Homan KA; Cook JR; Emelianov SY; Ermilov SA Co-registered photoacoustic and fluorescent imaging of a switchable nanoprobe based on J-aggregates of indocyanine green." Proc. SPIE 10494, Photons Plus Ultrasound: Imaging and Sensing 2018.

(14). Kim S; Shi Y; Kim JY; Park K; Cheng JX Overcoming the barriers in micellar drug delivery: Loading efficiency, in vivo stability, and micelle-cell interaction. Expert Opin. Drug Delivery 2010, 7, 49–62.

(15). (a)Chen F; Hong H; Shi S; Goel S; Valdovinos HF; Hernandez R; Theuer CP; Barnhart TE; Cai W Engineering of hollow mesoporous silica nanoparticles for remarkably enhanced tumor active targeting efficacy. Sci. Rep 2014, 4, 5080. [PubMed: 24875656] (b)Guardado-Alvarez TM; Chen

W; Norton AE; Russell MM; Connick WB; Zink JI Analyte-responsive gated hollow mesoporous silica nanoparticles exhibiting inverse functionality and an AND logic response. Nanoscale 2016, 8, 18296–18300. [PubMed: 27779267]

(16). (a)He Q; Zhang Z; Gao F; Li Y; Shi J In vivo biodistribution and urinary excretion of mesoporous silica nano-particles: Effects of particle size and PEGylation. Small 2011, 7, 271–280. [PubMed: 21213393] (b)Liu J; Luo Z; Zhang J; Luo T; Zhou J; Zhao X; Cai K Hollow mesoporous silica nanoparticles facilitated drug delivery via cascade pH stimuli in tumor microenvironment for tumor therapy. Biomaterials 2016, 83, 51–65. [PubMed: 26773665]

(17). (a)Li Y; Li N; Pan W; Yu Z; Yang L; Tang B Hollow mesoporous silica nanoparticles with tunable structures for controlled drug delivery. ACS Appl. Mater. Interfaces 2017, 9, 2123–2129. [PubMed: 28004570] (b)Chakravarty R; Goel S; Hong H; Chen F; Valdovinos HF; Hernandez R; Barnhart TE; Cai W Functionalized hollow mesoporous silica nanoparticles for tumor vasculature targeting and PET image-guided drug delivery. Nanomedicine (London, U. K.) 2015, 10, 1233–1246.(c)Luo Z; Hu Y; Cai K; Ding X; Zhang Q; Li M; Ma X; Zhang B; Zeng Y; Li P; Li J; Liu J; Zhao Y Intracellular redox-activated anticancer drug delivery by functionalized hollow mesoporous silica nanoreservoirs with tumor specificity. Biomaterials 2014, 35, 7951–7962. [PubMed: 24930850] (d)Du L; Liao S; Khatib HA; Stoddart JF; Zink JI Controlled-access hollow mechanized silica nanocontainers. J. Am. Chem. Soc 2009, 131, 15136–15142. [PubMed: 19799420]

(18). (a)Singh RK; Kim TH; Mahapatra C; Patel KD; Kim HW Preparation of self-activated fluorescence mesoporous silica hollow nanoellipsoids for theranostics. Langmuir 2015, 31, 11344–11352. [PubMed: 26393922] (b)Yang S; Chen D; Li N; Xu Q; Li H; Gu F; Xie J; Lu J Hollow mesoporous silica nanocarriers with multifunctional capping agents for in vivo cancer imaging and therapy. Small 2016, 12, 360–370. [PubMed: 26618618] (c)Huang CC; Huang W; Yeh CS Shell-by-shell synthesis of multi-shelled mesoporous silica nanospheres for optical imaging and drug delivery. Biomaterials 2011, 32, 556–564. [PubMed: 20875684] (d)Fan Z; Li D; Yu X; Zhang Y; Cai Y; Jin J; Yu J AIE luminogenfunctionalized hollow mesoporous silica nanospheres for drug delivery and cell imaging. Chem. - Eur. J 2016, 22, 3681–3685. [PubMed: 26711307]

(19). Hong S; Kim H; Choi Y Indocyanine green-loaded hollow mesoporous silica nanoparticles as an activatable theranostic agent. Nanotechnology 2017, 28, 185102. [PubMed: 28393763]

(20). (a)Soppera O; Turck C; Lougnot DJ Fabrication of micro-optical devices by self-guiding photopolymerization in the near IR. Opt. Lett 2009, 34, 461–463. [PubMed: 19373341] (b)Bonardi AH; Dumur F; Grant TM; Noirbent G; Gigmes D; Lessard BH; Fouassier J-P; Lalevee J Higher performance near-infrared (NIR) photoinitiating systems operating under low light intensity and in the presence of oxygen. Macromolecules 2018, 51, 1314–1324.

(21). Leung KCF; Nguyen TD; Stoddart JF; Zink JI Supramolecular nanovalves controlled by proton abstraction and competitive binding. Chem. Mater 2006, 18, 5919–5928.

(22). (a)Zhou W; Dridi M; Suh JY; Kim CH; Co DT; Wasielewski MR; Schatz GC; Odom TW Lasing action in strongly coupled plasmonic nanocavity arrays. Nat. Nanotechnol 2013, 8, 506–511. [PubMed: 23770807] (b)Yang A; Hoang TB; Dridi M; Deeb C; Mikkelsen MH; Schatz GC; Odom TW Real-time tunable lasing from plasmonic nanocavity arrays. Nat. Commun 2015, 6, 6939. [PubMed: 25891212]

(23). Oseledchyk A; Andreou C; Wall MA; Kircher MF Folate-targeted surface-enhanced resonance Raman scattering nanop-robe ratiometry for detection of microscopic ovarian cancer. ACS Nano 2017, 11, 1488–1497. [PubMed: 27992724]

(24). Berezin MY; Zhan C; Lee H; Joo C; Akers WJ; Yazdanfar S; Achilefu S Two-photon optical properties of near-infrared dyes at 1.55 μm excitation. J. Phys. Chem. B 2011, 115, 11530–11535. [PubMed: 21866928]

(25). Wang C; Weiss EA Sub-nanosecond resonance energy transfer in the near-infrared within self-assembled conjugates of PbS quantum dots and cyanine dye J-aggregates. J. Am. Chem. Soc 2016, 138, 9557–9564. [PubMed: 27359272]

(26). (a)Chen W; Tsai PH; Hung Y; Chiou SH; Mou CY Nonviral cell labeling and differentiation agent for induced pluripotent stem cells based on mesoporous silica nanoparticles. ACS Nano 2013, 7, 8423–8440. [PubMed: 24063246] (b)Chou CC; Chen W; Hung Y; Mou CY Molecular

elucidation of biological response to mesoporous silica nanoparticles in vitro and in vivo. ACS Appl. Mater. Interfaces 2017, 9, 22235–22251. [PubMed: 28608695] (c)Chen W; Cheng CA; Zink JI Spatial, temporal, and dose control of drug delivery using noninvasive magnetic stimulation. ACS Nano 2019, 13, 1292–1308. [PubMed: 30633500] (d)Zhang Y; Ang CY; Li M; Tan SY; Qu Q; Luo Z; Zhao Y Polymer-coated hollow mesoporous silica nanoparticles for triple-responsive drug delivery. ACS Appl. Mater. Interfaces 2015, 7, 18179–18187. [PubMed: 26221866]

(27). Modification of pores with APTS is predicted to have a size change of 0.5 nm, whereas we did not observe pore size change. See ref 26.

(28). (a)Rurack K; Spieles M Fluorescence quantum yields of a series of red and near-infrared dyes emitting at 600−1000 nm. Anal. Chem 2011, 83, 1232–1242. [PubMed: 21250654] (b)Hatami S; Würth C; Kaiser M; Leubner S; Gabriel S; Bahrig L; Lesnyak V; Pauli J; Gaponik N; Eychmüller A; Resch-Genger U Absolute photoluminescence quantum yields of IR-26 and IR-emissive $Cd_{1-x}Hg_xTe$ and PbS quantum dots- method and material-inherent challenges. Nanoscale 2015, 7, 133–143. [PubMed: 25407424]

(29). A sulfonated variant of the IR-140 chromophore has been characterized to J-aggregate in solution. See:(a)Berlephsch HV; Bottcher C Cryo-transmission electron microscopy reveals mesoscopic H- and J-aggregates of near infrared cyanine dyes. J. Photochem. Photobiol. A 2010, 214, 16–21.(b)Deshmukh A; Koppel D; Chuang C; Cadena D; Cao J; Caram JR Design principles for two-dimensional molecular aggregates using Kasha's model: tunable photophysics in near and short-wave infrared. J. Phys. Chem. C 2019, DOI: 10.1021/acs.jpcc.9b05060.

(30). NIR fluorophores have emission that extends into the SWIR.(a)Carr JA; Franke D; Caram JR; Perkinson CF; Saif M; Askoxylakis V; Datta M; Fukumura D; Jain RK; Bawendi MG; Bruns OT Shortwave infrared fluorescence imaging with the clinically-approved near-infrared dye indocyanine green. Proc. Natl. Acad. Sci. U. S. A 2018, 115, 4465–4470. [PubMed: 29626132] (b)Starosolski Z; Bhavane R; Ghaghada KB; Vasudevan SA; Kaay A; Annapragada A Indocyanine green fluorescence in second near-infrared (NIR-II) window. PLoS One 2017, 12, e0187563. [PubMed: 29121078] (c)Zhu S; Hu Z; Tian R; Yung BC; Yang Q; Zhao S; Kiesewetter DO; Niu G; Sun H; Antaris AL; Chen X Repurposing cyanine NIR-I dyes accelerates clinical translation of near-infrared-II (NIR-II) bioimaging. Adv. Mater 2018, 30, 1802546.

(31). Qiao Y; Polzer F; Kirmse H; Kirstein S; Rabe JP Nanohybrids from nanotubular J-aggregates and transparent silica nanoshells. Chem. Commun 2015, 51, 11980–11982.

(32). (a)Ruhle B; Saint-Cricq P; Zink JI Externally controlled nanomachines on mesoporous silica nanoparticles for biomedical applications. ChemPhysChem 2016, 17, 1769–1779. [PubMed: 26840996] (b)Chen W; Cheng CA; Lee BY; Clemens DL; Huang WY; Horwitz MA; Zink JI Facile strategy enabling both high loading and high release amounts of the water-insoluble drug Clofazimine using mesoporous silica nanoparticles. ACS Appl. Mater. Interfaces 2018, 10, 31870–31881 [PubMed: 30160469] (c)Chen W; Glackin CA; Horwitz MA; Zink JI Nanomachines and other caps on mesoporous silica nanoparticles for drug delivery. Acc. Chem. Res 2019, 52, 1531–1542. [PubMed: 31082188] (d)Cheng CA; Deng T; Lin FC; Cai Y; Zink JI Supramolecular nanomachines as stimuli-responsive gatekeepers on mesoporous silica nanoparticles for antibiotic and cancer drug delivery. Theranostics 2019, 9, 3341–3364. [PubMed: 31244957]

(33). (a)Sumer B; Gao J Theranostic nanomedicine for cancer. Nanomedicine 2008, 3, 137–140. [PubMed: 18373419] (b)Chakravarty R; Goel S; Hong H; Chen F; Valdovinos HF; Hernandez R; Barnhart TE; Cai W Hollow mesoporous silica nanoparticles for tumor vasculature targeting and PET image-guided drug delivery. Nanomedicine 2015, 10, 1233–1246. [PubMed: 25955122] (c)Ni D; Jiang D; Ehlerding EB; Huang P; Cai W Radiolabeling silica-based nanoparticles via coordination chemistry: basic principles, strategies, and applications. Acc. Chem. Res 2018, 51, 778–788. [PubMed: 29489335] (d)Zhao N; Yan L; Zhao X; Chen X; Li A; Zheng D; Zhou X; Dai X; Xu FJ Versatile types of organic/ inorganic nanohybrids: From strategic design to biomedical applications. Chem. Rev 2019, 119, 1666–1762. [PubMed: 30592420]

(34). (a)Brixner T; Hildner R; Kohler J; Lambert C; Wurthner F Exciton transport in molecular aggregates− From natural antennas to synthetic chromophore systems. Adv. Energy Mater 2017, 7, 1700236.(b)Doria S; Sinclair TS; Klein NF; Bennett DIG; Chuang C; Freyria FS; Steiner CP;

Foggi P; Nelson KA; Cao J; Aspuru-Guzik A; Lloyd S; Caram JR; Bawendi MG Photochemical control of exciton superradiance in light-harvesting nanotubes. ACS Nano 2018, 12, 4556–4564. [PubMed: 29701947]

(35). Kasha M; Rawls HR; El-Bayoumi MA The exciton model in molecular spectroscopy. Pure Appl. Chem 1965, 11, 371–392.

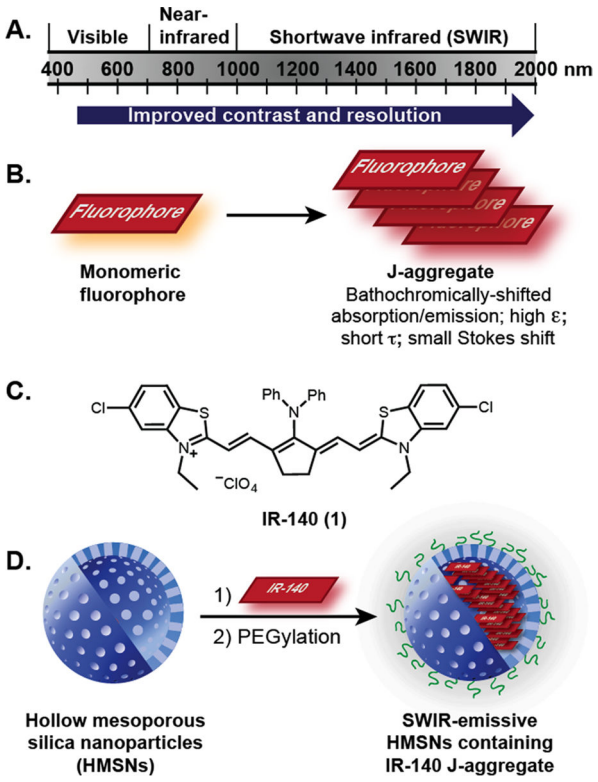

Figure 1.

(A) Regions of the electromagnetic spectrum employed for optical imaging. For further details on contrast and resolution within regions of the SWIR, see references 1b, 1c, 8b, 8c. (B) J-Aggregation and characteristic photophysical properties. (C) IR-140. (D) Work reported herein: the stabilization of IR-140 J-aggregates in hollow mesoporous silica nanoparticles (HMSNs) to result in biocompatible SWIR-emissive contrast agents.

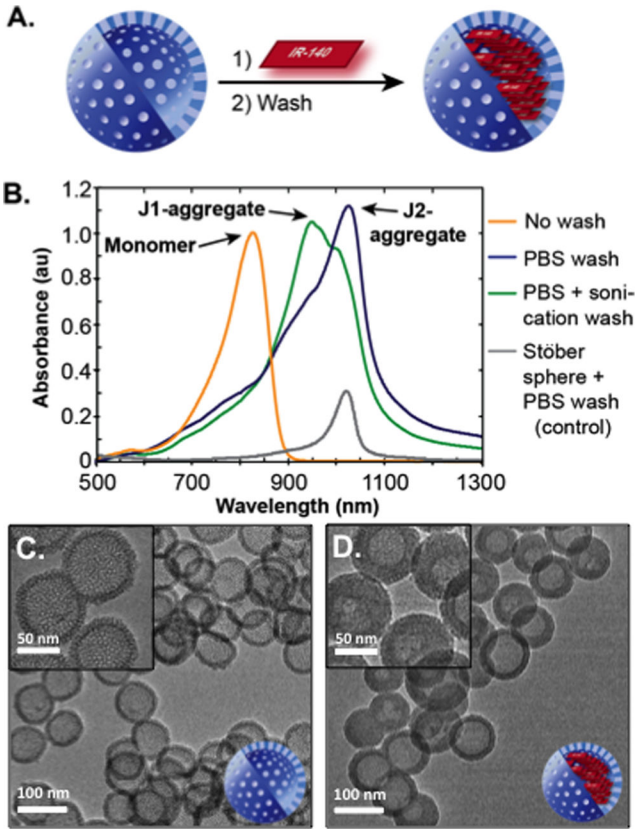

Figure 2.

(A) Schematic of loading IR-140 into HMSNs. (B) Washing conditions facilitate J-aggregation. 10 mg/mL HMSNs were combined with 10 mM IR-140 in DMSO and washed with PBS with (green) and without (dark blue) sonication. Prewash spectrum, diluted 1:350 is shown in orange. Loading control for solid, nonporous Stöber spheres is shown in gray. (C,D) TEM images of HMSNs with (D) and without (C) IR-140 treatment.

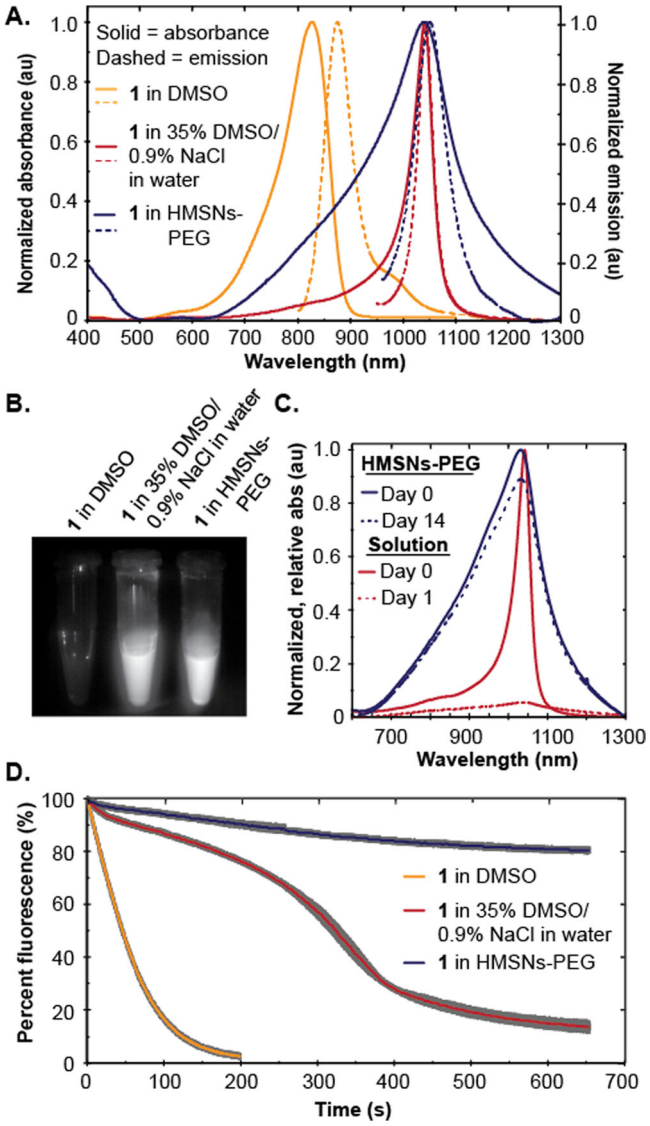

Figure 3.

(A) Normalized absorption and emission of IR-140 J-aggregate in HMSNs-PEG (blue), J-aggregate in solution (red), and monomer (yellow). (B) Emission (1000–1700 nm) of IR-140 monomer (left), J-aggregate in solution (middle) and J-aggregate in HMSNs-PEG (right) upon 980 nm excitation. (C) Normalized relative absorption of IR-140 J-aggregate in 35% DMSO/0.9% NaCl in water (red) and in HMSNs-PEG in PBS (blue) on day zero (solid) and day 1 or 14 (dotted). (D) Photostability under laser irradiation (97 mW/cm^2) at 980 nm for IR-140 J-aggregate in HMSNs-PEG (blue) and IR-140 J-aggregate in 35% DMSO/0.9–% NaCl in water (red), and at 785 nm for monomer in DMSO (yellow).

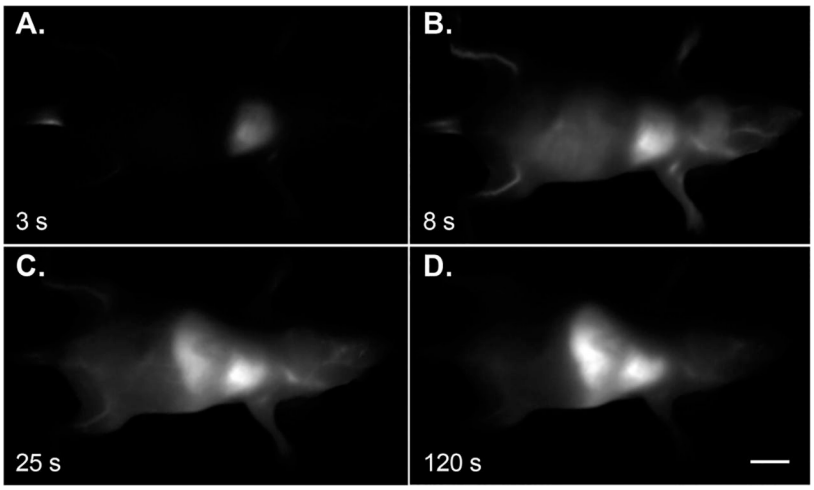

Figure 4.

Whole-mouse imaging at 16 fps (980 nm, 91 mW/cm^2 excitation; 1000–1700 nm collection) upon i.v. delivery of IR-140 HMSNs-PEG. Background subtracted stills were averaged over 5 frames at 3 s (A), 8 s (B), 25 s (C), and 120 s (D) postinjection. Scale bar represents 1 cm. Data are representative of two replicate experiments.